TOWARDS NEW V&V IN AOCS/GNC FOR INDUSTRIAL EFFICIENCY

Maurice Martin[(1)], Stefan Winkler[(1)], Frederik Belien[(1)], Roger Förstner[(2)]

[(1)]*Airbus Defence and Space GmbH, Claude-Dornier-Str., 88090 Immenstaad, Germany, maurice.martin@airbus.com*

[(2)]*Universität der Bundeswehr München, Neubiberg, Bayern, 85577, Germany*

ABSTRACT

This paper presents an enhanced verification and validation (V&V) framework that allows assessing the robust stability and performance of uncertain systems. Although robustness analysis techniques have been available for decades, they have not been integrated into the default industrial processes. To facilitate the use of robustness analysis techniques, a step-by-step approach has been developed.

The framework combines various V&V techniques including worst-case analysis, sensitivity analysis, and optimization within both the time and frequency domain. The outcome of the framework is the worst-case stability/performance metric and the ranking of the most influential uncertainties that cause the metric degradation. To illustrate the steps in the framework, the V&V techniques are applied on the normal mode of the satellite MetOp-SG (SAT-B). The results show that the worst case is efficiently found by avoiding time consuming simulations.

This implies that time and costs in the V&V procedure can be reduced through tailored V&V tools, which help to analyze complex AOCS/GNC systems efficiently.

1 INTRODUCTION

Current and future space missions require increasingly more complex AOCS/GNC designs for stringent performance requirements. At the same time, the cost and time constraints for missions scale at a smaller rate compared to the complexity. This gap between increased complexity and mission time and cost constraints are tackled through industrial efficient in the established V&V procedures.

The default method for V&V of AOCS/GNC systems are Monte Carlo (MC) simulation campaigns. Uncertainties in the system are randomly sampled and the variations in the outputs are analyzed and compared to a given requirement. The major benefit of this approach is its easy implementation, its applicability to any kind of system, and the probability assessment of given requirements. This comes at the cost of large amount of time-consuming simulations, missing the worst-case scenario, and giving no insights into the system drivers.

To tackle the drawbacks of the default method, an alternative approach based on worst-case analysis is proposed. The new framework relies on various V&V techniques including robustness analysis based on μ-analysis [1], sensitivity analysis, and optimization. It shifts most of the V&V activities from the time to the frequency domain. This saves time because frequency analysis can be faster than in the time domain. By combining robustness and sensitivity analyses, it is possible to not only find the worst-case scenario, but also to identify the uncertainties that are driving the system's performance degradation. The added benefit from this new V&V framework is demonstrated on a realistic case study based on the MetOp-SG (SAT-B) in its normal mode.

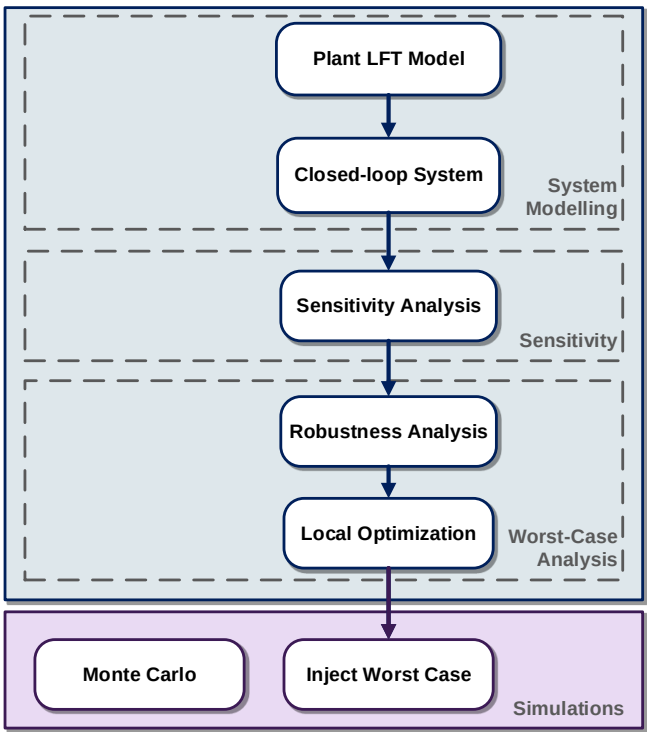

Figure 1: Overview of the enhanced V&V framework.

The paper is structured as follows. In section 2, the new V&V framework is presented. In section 3, the MetOp-SG (SAT-B) is introduced and the V&V problem is formulated. In section 4, the application of the V&V framework on the MetOp-SG (SAT-B) example is demonstrated. Finally, conclusions are given in section 5.

2 ENHANCED V&V FRAMEWORK

The enhanced V&V framework consists of four steps as illustrated in Figure 1. Firstly, the uncertain closed loop system has to be modeled using the linear fractional transform (LFT) framework. This includes the kinematics and dynamics of the plant and any other relevant dynamical parts of the closed loop system. Secondly, a sensitivity analysis is conducted to identify the uncertainties that degrade the stability and performance metrics the most. Thirdly, a robustness analysis is conducted to determine the worst-case parameter combination for each metric. Lastly, this worst-case is inserted into a simulator. The results can be compared to the default method of conducting Monte Carlo simulation campaigns directly. Details of the first three steps are given in the following.

2.1 System Modelling

The enhanced V&V framework analyses a control loop given in form of the standard formulation shown in Figure 2. The plant dynamics $G(s)$ are interconnected with the controller $K(s)$ in a feedback loop. This closed-loop system is excited by noise n and disturbances d. These inputs are propagated through the closed-loop system to the outputs of interest. Typically, these are the attitude errors e and control effort u. In this paper, only the attitude error is analyzed.
To obtain a physical representation of the inputs shaping filters $W_n(s)$, $W_d(s)$ are introduced. Under the assumption that the inputs w_n, w_d are stationary random processes in form of unity white noise, their frequency content is properly defined by their power spectral density (PSD). The output

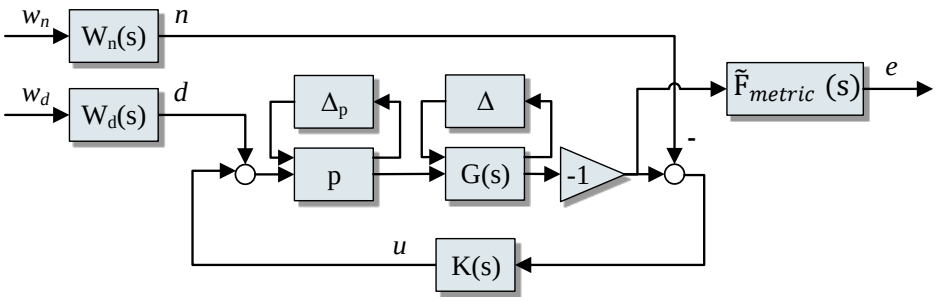

Figure 2: Standard formulation of the control loop for the enhanced V&V framework.

is weighted according to the specified performance metric. In attitude control problems, there are standardized metrics that describe (windowed) attitude errors such as, among others, absolute pointing error (APE) and relative pointing error (RPE). In [2], [4], [5] the exact weighting functions have been derived for the various metrics. These have been expressed as rational shaping filters $\tilde{F}_{metrics}(s)$ summarized in [8].
To include uncertainties in the control loop the nominal plant is extended to an uncertain plant through the LFT framework. In Figure 2, the uncertainties of the plant are presented by Δ. An input perturbation p is introduced for stability analysis problems. The corresponding uncertainty Δ_p allows assessing how large this perturbation can be until the closed-loop system becomes unstable.

2.2 Sensitivity Analysis

Whereas the robustness analysis quantifies how large the worst-case stability and performance metric is, sensitivity analysis quantifies the influence of each uncertainty to the metric degradation. These two analyses are combined to take advantages of each method. First, the sensitivity analysis is conducted to rank the influence of each uncertainty. This information is used to reduce the complexity of the plant LFT model. The *full* LFT model is reduced to a *sesnsitive* LFT model by removing insensitive uncertainties from the model. This greatly reduces the computational time of the robustness analysis. Additionally, the information is helpful for identifying system drivers. The design can be improved by reducing the uncertainty range of the sensitive parameters.
In the enhanced V&V framework, the sensitive uncertainties are identified using the elementary effect (EE) metric from the field of global sensitivity analysis (GSA). The term *global* implies that the whole uncertainty space is explored. In contrast, *local* techniques are limited to analysis around a given point in the uncertainty space. The EE extends the idea of finite difference to the global uncertainty space. Let $y = f(\Delta)$ be a generic function for the computation of the stability and performance metrics for a given uncertainty sample of the plant Δ_j, then the EE is defined as [7]:

$$\delta y_{i,j}^{EE} = \frac{f(\Delta_j + k_{i,j}\mathbf{e}_i) - f(\Delta_j)}{k_{i,j}} \tag{1}$$

where $i = \{1, \ldots, n\}$ is the i-th uncertainty, $j = \{1, \ldots, r\}$ is the number of picked samples, $\mathbf{e}_i$ is the i-th canonical vector, and $k_{i,j}$ is the size of the perturbation.
The sensitivity metric used in the enhanced V&V framework is the absolute mean value over all samples:

$$\delta y_i^{EE} = E\{|\delta y_{i,j}^{EE}|\} \tag{2}$$

Hence, there is one sensitivity metric per uncertainty. The larger the sensitivity metric is the more influence it has on stability and performance metrics. The uncertainties are ranked from most sensitive

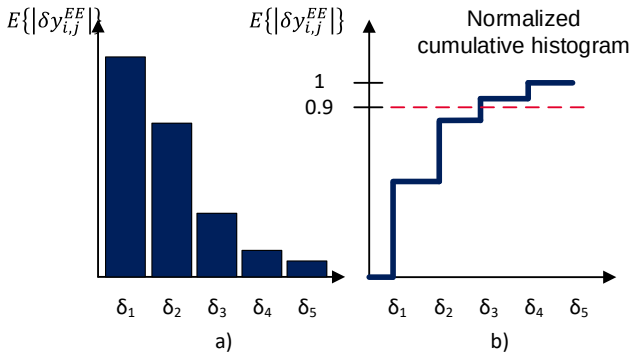

Figure 3: Sorting of most sensitive uncertainties by the elementary effect.

to least sensitive by sorting their corresponding sensitivity metric in form of a histogram. An example of this ranking is shown in Figure 3 a). Alternatively, the ranking can be represented by a normalized cumulative histogram. This representation is utilized to define a threshold between sensitive and insensitive uncertainties. In Figure 3 b), a threshold is set at 90%, so that only two uncertainties are considered instead of five.
In case of uncertain systems represented as LFTs, the function evaluation in (1) consists of simply substituting the LFT with the picked sample and evaluating the stability or performance of the resulting linear time-invariant (LTI) system.

2.3 Robust Stability Analysis

The most commonly used stability metrics are the gain, phase, and modulus margins in the AOCS/GNC domain. The choice of the margin influences the type of input perturbation in Figure 2. The stability margins can be computed directly from the open loop system and sensitivity function for a nominal system, i.e. no uncertainties. The computation does not require the inputs and outputs of the interconnection in Figure 2, because it is an inherent property of the linear system. When plant uncertainties are introduced, the margins are expected to degrade to lower values. To quantify this degradation, the problem can be recast as a skewed μ-analysis [9]. It splits the uncertainty space into the plant uncertainties Δ and perturbation uncertainties Δ_p. The plant uncertainties are fixed to lie within a predefined size, whereas the perturbation uncertainty is scaled until the system becomes unstable. The LFT formulation of the gain, phase, and modulus margin perturbation is given by:

$$p_{gm} = 1 + \delta_r = F_u\left(\begin{bmatrix} 0 & 1 \\ 1 & 1 \end{bmatrix}, \delta_r\right) \tag{3}$$

$$p_{pm} = e^{j\phi} = \frac{1 - j\delta_r}{1 + j\delta_r} = F_u\left(\begin{bmatrix} -j & -2\sqrt{j} \\ \sqrt{j} & 1 \end{bmatrix}, \delta_r\right) \tag{4}$$

$$p_{mm} = 1 + \delta_c = F_u\left(\begin{bmatrix} 0 & 1 \\ 1 & 1 \end{bmatrix}, \delta_c\right) \tag{5}$$

where $\delta_r \in \mathbb{R}$, $\delta_c \in \mathbb{C}$ and $F_u(M, \Delta)$ is the shorthand notation for the upper LFT. Solvers for this kind of problem are given in [16].
The stability of the system could also be analysed using the robust stability analysis of the μ-analysis directly. In this analysis, no input perturbation is assumed, but the size of the plant uncertainty is increased until the closed-loop system becomes unstable. Although this is useful additional information, most stability requirements are given as margins. Therefore, it is not used in this paper.

2.4 Robust Performance Analysis

Performance analyses are conducted for specific channels of the closed-loop system. Using the interconnection in Figure 2, the input and output relations are expressed in terms of the complementary sensitivity function $T(s)$ and sensitivity function $S(s)$:

$$\mathbf{e} = \underbrace{\begin{bmatrix}\tilde{\mathbf{F}}_{metric}\mathbf{T}\mathbf{W}_n & -\tilde{\mathbf{F}}_{metric}\mathbf{F}_u(\mathbf{G},\Delta)\mathbf{S}\mathbf{W}_d\end{bmatrix}}_{\mathbf{H}_e(s)} \begin{pmatrix}\mathbf{w}_n \\ \mathbf{w}_d\end{pmatrix} \tag{6}$$

Note that the input perturbation p is disregarded for this analysis and the Laplace variable argument is left out for brevity.
In the AOCS/GNC domain performance metrics are commonly given in form of PSDs or the (windowed) attitude error metrics. The PSD requirement can be directly analysed using the robust performance (RP) analysis of the μ-analysis. In [1], [3], it is shown that the RP μ-analysis is equivalent to the H_∞-norm:

$$\max_{\Delta\in\mathbf{\Delta}} \|F_u(\mathbf{H}_{zw}(j\omega),\Delta)\|_\infty < \gamma \tag{7}$$

where $\mathbf{H}_{zw}(s)$ is a given transfer function from w to z, γ is the robust H_∞-norm, and the uncertainty is confined to the unit ball $\mathbf{B}_{\mathbf{\Delta}} = \{\Delta(s) \in \mathbf{\Delta} : \|\Delta\|_\infty \leq 1\}$. In terms of the interconnection in Figure 2, the transfer function is chosen according to one (or several) performance channels in (6). The output filter $\mathbf{F}_{metric}(s)$ is can be set as the inverse of the PSD requirement, if a proper and stable rational expression exists. In this case, it is sufficient to show that the robust H_∞-norm of (7) is less than one [11]. Alternatively, the output filter is set to unity, then the resulting robust H_∞-norm per frequency point has to be compared to the given PSD requirement.
The second performance type is the (windowed) attitude error metrics. In [10], it is shown that this metric can be evaluated using the H_2-norm. In the frequency domain, it can be interpreted as the integral over the system magnitude. In the following, a single input single output (SISO) system is assumed for the robust H_2-norm definition.

$$\|F_u(H_{zw},\Delta)\|_2 := \max_{\Delta\in\mathbf{\Delta}} \left(\frac{1}{2\pi}\int_{-\infty}^{\infty} |F_u(H_{zw}(j\omega),\Delta)|^2 d\omega\right)^{1/2} \tag{8}$$

The magnitude of the LFT in equation (8) is replaced by the robust performance μ-problem of equation (7) for each frequency point [14].

$$\|F_u(H_{zw},\Delta)\|_2 \leq \left(\frac{1}{2\pi}\int_{-\infty}^{\infty} \max_{\Delta\in\mathbf{\Delta}} \|F_u(H_{zw}(j\omega),\Delta)\|_\infty^2 \, d\omega\right)^{1/2} \tag{9}$$

The equation (9) is an upper bound with respect to (8), because the magnitude of the transfer function is maximized for each frequency point. This results in possibly multiple worst cases for each frequency point, whereas equation (8) only has one worst case for the whole integral. The integral is computed numerically, whose error is minimized using an adaptive integration scheme.

2.5 Local Optimization

The major drawback of utilizing the sensitive LFT is that not all uncertainties are considered in the robust stability and performance analyses. To recover the effect of the neglected uncertainties, a local

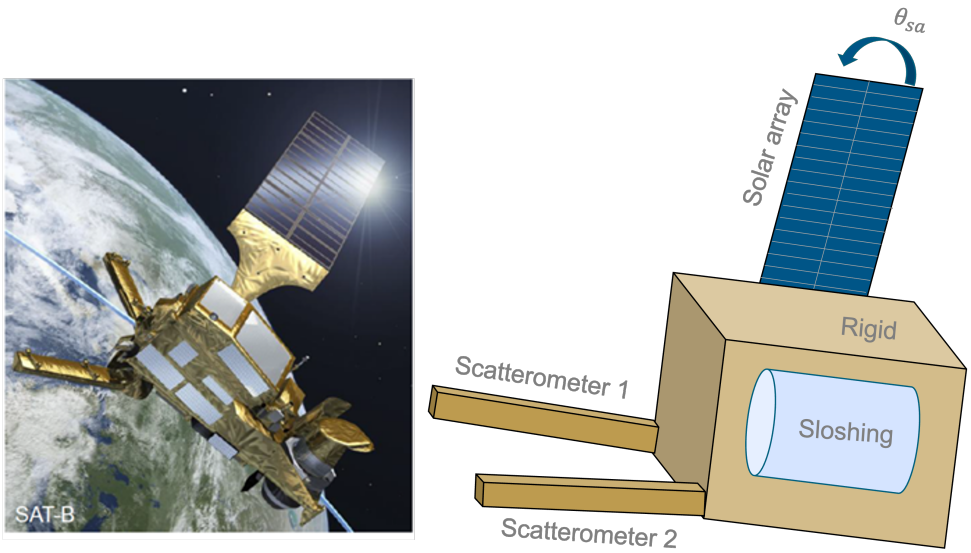

Figure 4: Artistic illustration of MetOp-SG SAT-B (left) adjusted from [15], and multi-body model (right).

optimization on the robustness metric is performed based on the sequential quadratic programming (SQP) method:

$$\begin{aligned} &\min_{\mathbf{x}\in\Delta} f(\mathbf{x}) \\ \text{subject to } &-1 \leq x_i \leq 1 \end{aligned} \tag{10}$$

The meaning of $f(\mathbf{x})$ is equivalent to elementary effect definition in (1). Note that for performance metrics the minimum has to be changed to a maximum to obtain the worst case.
The initial guess is the worst-case parameter configuration obtained from the robust stability and performance metrics in the section 2.3 and 2.4. This analysis uses the sensitive LFT, so that only worst-case parameters for the sensitive uncertainties are available. The initial value of all insensitive values are set to zero (nominal value).

3 METOP-SG PROBLEM FORMULATION

3.1 Mission Description

The enhanced V&V framework is demonstrated on the MetOp-SG SAT-B satellite, which includes a vast range of uncertainties and slowly time-varying parameters throughout the mission. The satellite is planned to fly in a Sun-synchronous orbit around the Earth at a mean altitude of about $835\,\mathrm{km}$. In the normal mode, its attitude is mainly nadir pointing towards the Earth. In this mode it uses star trackers (STRs) to determine its attitude and reaction wheels as actuators. A subset of stability and performance requirements for this mode are summarized in Table 1.

3.2 Closed-loop Model for normal mode

The MetOp-SG SAT-B satellite is modeled as a multi-body consists of the central body (CB), solar array (SA), two SAs and fuel tank (F). An illustration of the multi-body model is given in Figure 4. The kinematics and dynamics of this system are modeled according to the Two-Input Two-Output Port (TITOP) from [13]. The central body and fuel tank are modeled as rigid bodies, and the solar array and scatterometers are flexible appendages. In this model, the central body is interconnected

Table 1: Stability and performance requirements.

Metric	Requirement
Gain margin	6 dB
Phase margin	30 deg
Modulus margin	0.5
APE	61.88 arcsec

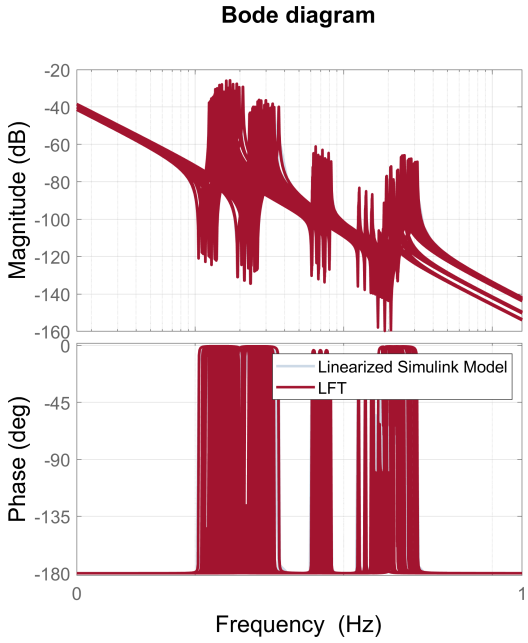

Figure 5: Bode diagram for the plant transfer function (x-axis) with normalized frequency axis.

with the appendages using feedback loops. Uncertainties are introduced for each component of the multi-body model resulting in LFTs for each component. It is possible to form one LFT out of all the LFT blocks using the LFT algebra [6]. The uncertainty block of the LFT has the size 72×72 with 20 uncertainties and there are 26 states. The inputs and outputs of the plant are the torques and attitude angles in the three axes.

The plant LFT is verified by comparing the frequency response of the LFT with linearized models from the nonlinear Simulink model. In Figure 5, the Bode diagram for the transfer function from the torque to the attitude angles for randomly sampled uncertainties are shown. The difference between the two models is indistinguishable, which indicates that the LFT model matches the linear behavior of the nonlinear simulator around the trim condition.

The described plant LFT is interconnected with the normal mode controller as shown in Figure 2. The attitude angles are feedback to the controller, which turns them into torque commands. The controller is a PID-based controller with various additional filters. The controller is designed to gain stabilize the flexible modes of the satellite for the normal mode. In this mode, the satellite points its instruments towards the Earth with high accuracy using STR and reaction wheels. The number of states of the controller are 28.

The noise and disturbance inputs to the system have to be described by the shaping filters $W_n(s)$, $W_d(s)$ for the performance analysis. The noise stems from the STR measurement error. The error model for the follows the standards given in [12], where the total noise consists of the summation of temporal, low spatial frequency error, and high spatial frequency error. The resulting shaping filter

Table 2: Uncertainties for the AOCS benchmark.

Uncertainty	Symbol	Range	Repetition
Central body mass	m_{cb}	10%	3
Central body MoI	J_{cb}	20%	6
SA mass	m_{sa}	10%	5
SA MoI	J_{sa}	20%	3
SCA (1) mass	m_{sca_1}	10%	5
SCA (1) MoI	J_{sca_1}	20%	3
SCA (2) mass	m_{sca_2}	10%	5
SCA (2) MoI	J_{sca_2}	20%	3
Fuel mass	m_f	23.2%	6
SADM angle	θ_{sadm}	$[-\pi, \pi]$	16
Cantilever frequency S/A	ω_{sa}	10%	12
Cantilever frequency SCA1	ω_{sca_1}	10%	4
Cantilever frequency SCA2	ω_{sca_2}	10%	4

Table 3: Sensitive uncertainties for the stability metrics.

	Gain margin	Phase margin	Modulus margin
x-axis	J_{sa}, θ_{sadm}, J_{cb}, m_{sa}, m_{sca_1}	J_{sa}, J_{cb}, θ_{sadm}, m_{sa}, m_{sca_1}	J_{sa}, J_{cb}, m_{sa}, θ_{sadm}, m_{sca_1}
y-axis	J_{cb}, m_f, m_{cb}	J_{cb}, m_f, θ_{sadm}, m_{sca_1}	J_{cb}, m_f, θ_{sadm}, m_{sca_1}
z-axis	J_{cb}, J_{sa}, θ_{sadm}, m_f, J_{sca_2}, J_{sca_1}	J_{cb}, J_{sa}, θ_{sadm}, m_f, m_{sca_2}, J_{sca_2}	J_{cb}, J_{sa}, θ_{sadm}, m_f, J_{sca_1}, m_{sca_1}

Table 4: Sensitive uncertainties for the performance metrics.

	APE for $\mathbf{H}_e(s)$
x-axis	J_{sa}, J_{cb}, m_{sa}, J_{sca_2}
y-axis	J_{cb}, m_f, m_{cb}
z-axis	J_{cb}, J_{sa}, m_f, m_{sa}, J_{sca_1}

$W_n(s)$ has a size of 3×9 with 6 states. The disturbances are external torques from the environment. The model includes effects from aerodynamic drag, gravity gradient torque, magnetic torque, and solar radiation pressure. The resulting shaping filter $W_d(s)$ has a size of 3×12 with 21 states.

4 WORST-CASE ANALYSIS

4.1 Sensitivity Analysis

In the sensitivity analysis, the uncertainties defined in Table 2 that mostly affect the stability and performance metrics from Table 1 are identified according to the method described in 2.2. The sensitivity analysis requires a predefined number of samples r according to (1), which is chosen to be 50. These samples are perturbed for each uncertainty resulting in $r(n+1) = 1050$ total function evaluations.

The most sensitive uncertainties within 90% of the cumulative histogram, see example in Figure 3, are summarized for stability and performance metrics in Table 3 and Table 4 respectively. For illustrative purposes, the cumulative histogram for the performance channel in the x-axis is shown in Figure 6. In this example, the moment of inertia (MoI) of the SA J_{sa} has the largest sensitivity metric, whose value is roughly 46% of the summation of all sensitivity metrics combined. There are three more uncertainties (J_{cb}, m_{sa}, m_{sca_1}) that contribute up to 90% of the total. Therefore, four uncertainties are identified as sensitive according to Table 4. The same procedure is conducted for the other axes and stability metrics.

The result of the sensitivity analysis indicates various properties of the system. Firstly, the tables reveal that most of the sensitive parameters belong to the mass and MoI of the various multi-bodies. The cantilever frequencies do not appear as sensitive uncertainties. This is a reasonable result, because the controller suppresses the flexible modes through gain stabilization, i.e. the controller does not react to high frequency excitations. Thus, the contribution of the flexible modes on the stability and performance is negligible.

Secondly, the mass uncertainties also influence the attitude system. It changes the MoI of the multi-body system because of the parallel axis theorem which includes the mass:

$$\mathbf{J}^A = \mathbf{J}^B + m\left(\tilde{\mathbf{r}}^{BA}\right)^T \tilde{\mathbf{r}}^{BA} \tag{11}$$

for two arbitrary reference points A and B and a torque arm $\mathbf{r}^{BA}$. The cross product matrix is indicated by the tilde. The central body has the largest MoI in terms of its principal axes for this particular example. Therefore, the central body uncertainty $\mathbf{J}_{cb}$ is expected to have a significant influence on the performance metrics. However, the arms of the appendages in the form of $\mathbf{r}^{BA}$ are large enough, so that masses of appendages also influence the MoI.

Thirdly, the solar array drive mechanism (SADM) angle is influential in almost all stability and performance channels. This is the result of the relatively large solar array compared to the central body. The torque arm is the largest for this appendage.

Lastly, the table shows that the number of uncertainties for the LFT can be reduced by more than half for both stability and performance analysis. The largest number of sensitive uncertainties are 6 compared to 20 for the full LFT. This helps to significantly reduce the computation time for the subsequent robustness analysis using the μ-analysis.

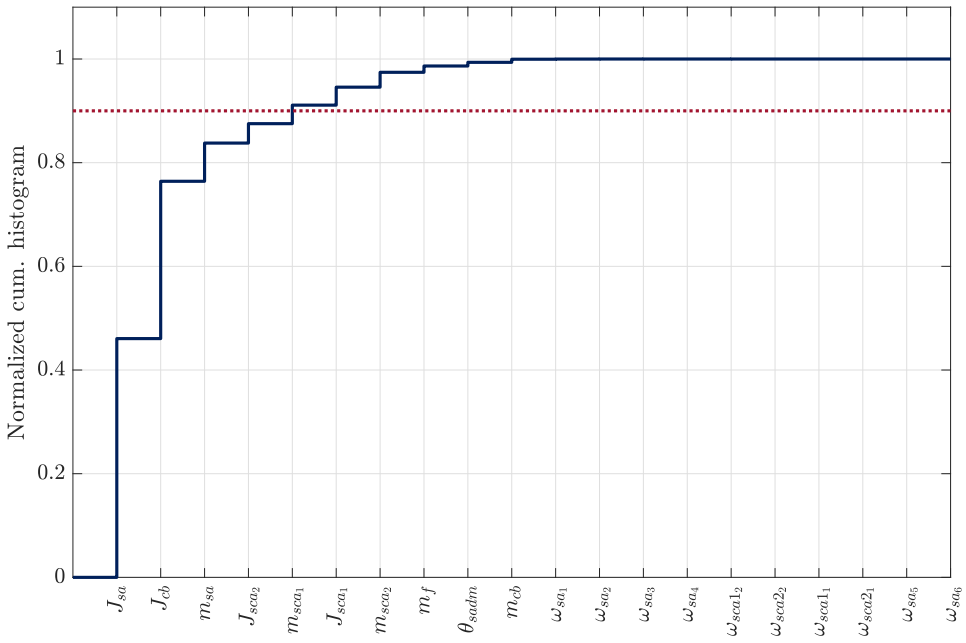

Figure 6: Normalized cumulative mean EE for the performance channel in the x-axis.

4.2 Robust Stability Analysis

Sensitive LFTs with a reduced number of uncertainties are created based on the sensitivity analysis results from Table 3. The μ-analysis is applied to the system to determine the robust gain, phase, and modulus margin according to section 2.3.
The results are summarized for each control axis in Table 5. The nominal values (fourth column) are the stability metrics when no uncertainties are present. The robust stability metrics (fifth column) are the result of the worst-case analysis using only the most sensitive uncertainties. The difference between the nominal and robust values shows the influence of the uncertainties on the margins. In this example, the uncertainties degrade the margins by around 1-2 dB and 1-3 deg. The requirements from Table 1 are still all met because of the relatively high nominal margins.
The results of the robust margins can be illustratively using the Nichols plot. In Figure 7, the nominal system response is shown as a solid blue line. By randomly sampling 1000 uncertainties from Table 2, this nominal response varies indicated by the solid grey lines. The variations are bounded by the worst-case stability margins. In this example, the gain and phase margins have two different worst-case parameter combinations and the worst-case modulus margin is equal to the gain margin. The worst-cases belong to the sixth column of Table 5, which is explained in more detail in section 4.4.

4.3 Robust Performance Analysis

Sensitive LFTs with a reduced number of uncertainties are created based on the sensitivity analysis results from Table 3. The μ-analysis is applied to the system to determine the robust performance metric according to section 2.4.
The results are summarized for each control axis in Table 6. The table is structured analogous to the stability metrics in Table 5. In this example, the uncertainties increase the APE metric only marginally by less than one arcsec. The results indicate a robust controller, which mets the requirements given in Table 1 with large margins.
The results of the robust margins can be illustratively using the cumulative single sided (SS) power spectrum (PS). It is the integration of the magnitude over the frequency according to (8) and (9). As

Table 5: Stability robustness metrics for the nominal and robust controllers

	Metric	Unit	Nominal	Robust	Robust (local optimization)
x-axis	Gain margin	[dB]	15.06	13.24	12.99
	Phase margin	[deg]	48.88	46.85	46.49
	Modulus margin	[-]	0.77	0.74	0.73
y-axis	Gain margin	[dB]	-15.25	-13.93	-13.77
	Phase margin	[deg]	47.68	45.10	44.64
	Modulus margin	[-]	0.78	0.76	0.76
z-axis	Gain margin	[dB]	11.28	9.75	9.53
	Phase margin	[deg]	50.51	49.49	49.16
	Modulus margin	[-]	0.71	0.66	0.65

Table 6: Performance robustness metrics.

	Metric	Unit	Nominal	Robust	Robust (local optimization)
x-axis	APE	[arcsec]	3.47	3.52	3.53
y-axis	APE	[arcsec]	3.09	3.17	3.18
z-axis	APE	[arcsec]	1.54	1.56	1.56

an example, the cumulative SS PS for the x-axis is visualized in Figure 8. The nominal system response is shown as a solid blue line and the perturbed system response using 1000 randomly sampled uncertainties is indicated by the solid grey lines. The upper (dashed red line) and lower (dotted green line) bounds belong to the μ-analysis for the robust H_2-norm. The lower bound values correspond to the fifth column of Table 6. The upper bound is always larger than the random samples, but the lower bound is smaller for some cases. The reason for this behavior is that the lower bound only considers the sensitive uncertainties, whereas the random samples consider all uncertainties in Table 2. This is improved by the local optimization detailed in the following section.

4.4 Local Optimization Analysis

The robustness analysis for the stability and performance based on the μ-analysis in the sections 4.2 and 4.3 only considered the sensitive uncertainties. To include the insensitive uncertainties, a local optimization is performed. The worst-case parameter combinations from robust metrics in the fifth column of Table 5 and Table 6 are used as an initial guess for the local optimizer. Insensitive uncertainties are set to their nominal value of zero. A maximum of 200 function evaluations is set for the SQP solver to limit the number of iterations.
The final values from the solver are the sixth columns of Table 5 and Table 6. In both tables, the optimizer finds slightly more degraded metrics compared to the robustness analysis with the sensitive uncertainties (fifth column). This degradation is not as large as the degradation between the nominal (fourth column) and robust (fifth column) values. This indicates that the sensitive LFTs are able to capture most of the metric degradation. The gap between column five and six could be reduced by setting a larger threshold for the sensitive uncertainties, e.g. increasing the threshold value from 90% to 95%.

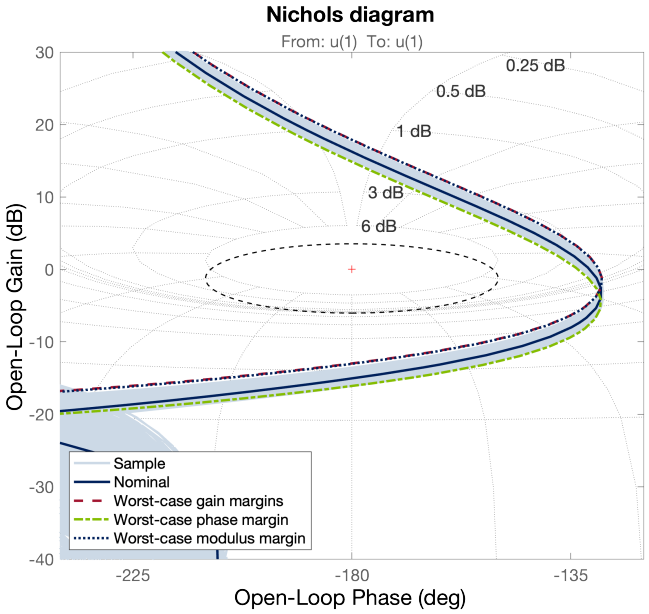

Figure 7: Worst-case stability margins for x-axis.

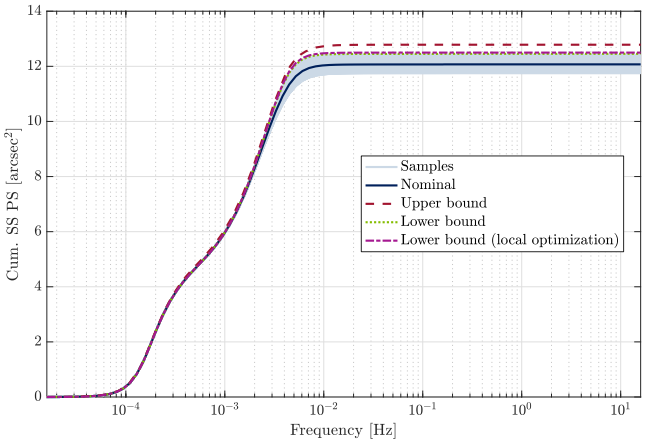

Figure 8: Worst-case attitude performance for $H_e(s)$ (x-axis).

The gap between the fifth (green dotted line) and sixth (purple dashed-dotted line) columns is very small for the example in Figure 8. After optimizing the lower bound from the fifth column of Table 6, the optimized lower bound (sixth column) is larger than the 1000 random samples. The corresponding worst-case parameter combinations are shown in Figure 9. The normalized values of the worst case are plotted in the y-axis for each uncertainty in the x-axis, which are sorted from most to least sensitive. The robustness analysis with the sensitive LFT only includes the four uncertainties, whereas the local optimizer considers all 20 uncertainties. The figure shows that the values of the sensitive uncertainties are unchanged. It mainly optimized all other masses and MoIs. Many of the cantilever frequencies are unaltered by the optimizer. This is reasonable because the flexible modes of the appendages are suppressed by the controller, so that they do not influence the performance metric.

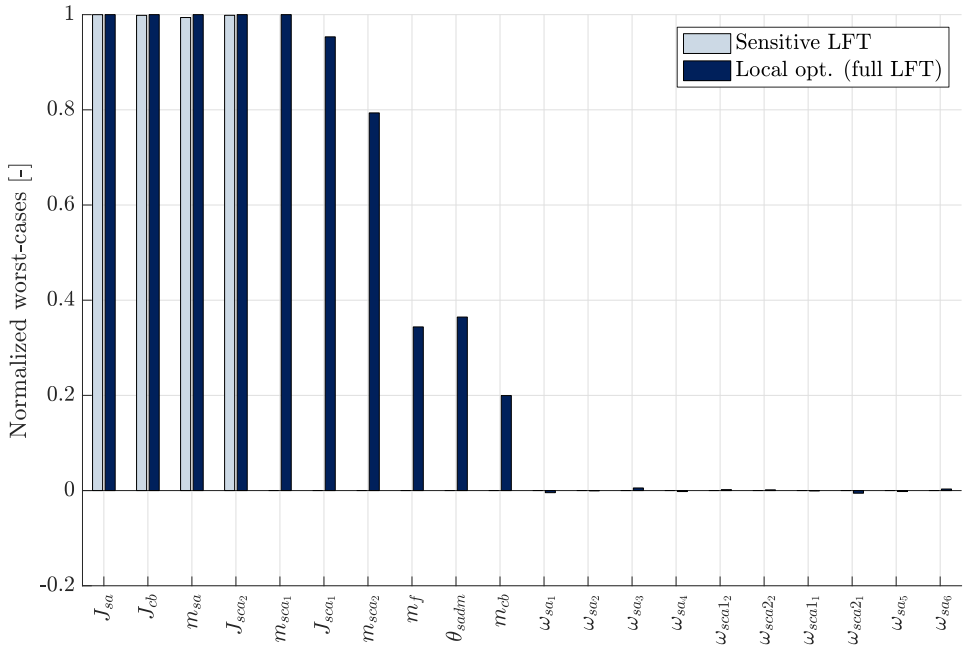

Figure 9: Worst-case parameter combination for $H_e(s)$ (x-axis).

4.5 Comparison with Monte Carlo Simulations

The alternative to the worst-case analysis from the enhanced V&V framework is to conduct Monte Carlo simulations directly on the nonlinear simulator. This comparison is shown for the performance metric. Compared to the frequency analysis, the simulations take a long time because low frequency content has to be simulated for the APE requirement, while at the same time high frequency content from the flexible modes are simulated.
In Figure 10, the results of 1000 Monte Carlo simulations are shown for the APE in the x-axis. Compared to the worst-case metric obtained from the enhanced V&V framework (sixth column in Table 6), the Monte Carlo metrics are always below the worst case. This result can be expected because the considered study case only has nonlinearities in the plant, which can be well represented by the linear plant LFT as shown in Figure 5.

5 CONCLUSION

The demonstration of the enhanced V&V framework on the MetOp-SG example has demonstrated a systematic approach to gain insights into the uncertain system behavior. The first step to better understand the system is to model the uncertain dynamics in form of a physical LFT. Unlike the numerical linearization method, the effect of uncertainties can be directly traced back to the LFT equations. This comes at the expense of increased modeling effort.
In the second step, the sensitivity analysis quantifies the effect of each uncertainty. This information is useful in multiple ways. The overall performance of the system can be enhanced by reducing the uncertainty range of the most sensitive parameters. For instance, this can be achieved through calibration before or during a mission. Additionally, the sensitivity analysis has been used to reduce the complexity of the LFT as shown in this paper. Instead of analyzing all 20 uncertainties, it has been shown that mainly six or less uncertainties are significantly affecting the system's performance. By reducing the LFT to the much smaller size, the μ-based robustness analysis is very efficient to find the worst cases. The worst-case analysis in the frequency domain helps to identify the frequency

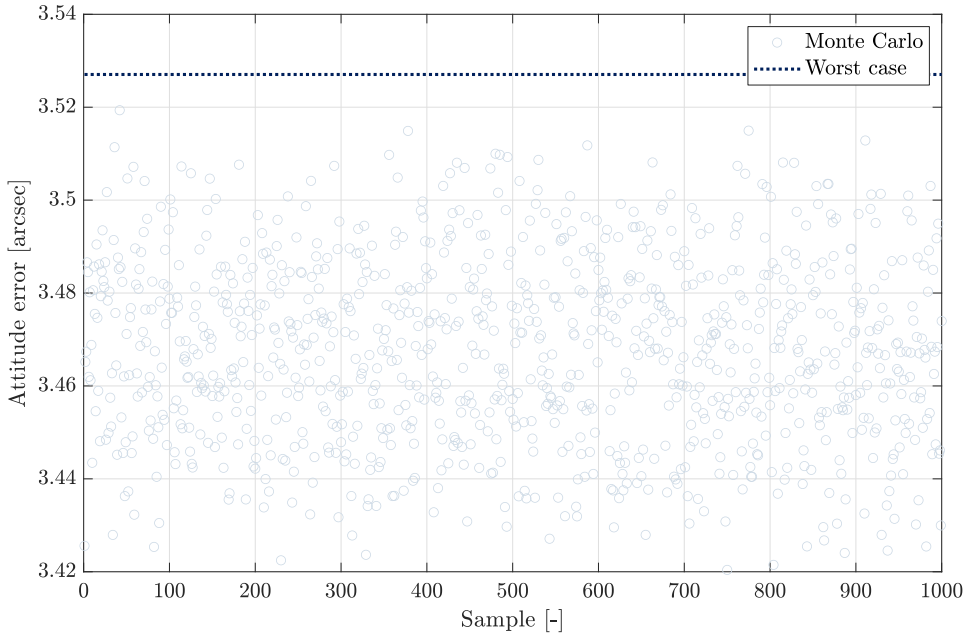

Figure 10: Worst-case Monte Carlo simulation (x-axis).

range in which the uncertainties affect the system the most. This information is useful to redesigned the controller if necessary.
In contrast, the worst-case metric found by the traditional MC analysis is smaller for all considered systems. Especially when the performance evaluation is very time-consuming (e.g. high-fidelity simulations), this method is not very efficient. Although it provides a probabilistic assessment of the worst-case performance, it gives no quantifiable insight, which uncertainty is driving the performance degradation.
The enhanced V&V framework is currently limited to linear problems such as the presented normal mode of MetOp-SG. Other modes, where for example transient and nonlinearities such as saturations are present, would require a different analysis approach.

REFERENCES

[1] J. Doyle, "Analysis of feedback systems with structured uncertainties," in *IEE Proceedings D Control Theory and Applications*, Institution of Electrical Engineers, vol. 129, 1982, pp. 242–250.

[2] R. L. Lucke, S. W. Sirlin, and A. M. San Martin, "New definitions of pointing stability-ac and dc effects," *Journal of the Astronautical Sciences*, vol. 40, no. 4, pp. 557–576, 1992.

[3] K. Zhou, J. Doyle, and K. Glover, *Robust and Optimal Control*, ser. Feher/Prentice Hall Digital and. Prentice Hall, 1996, ISBN: 9780134565675.

[4] M. E. Pittelkau, "Pointing error definitions, metrics, and algorithms," *Advances in the Astronautical Sciences*, vol. 116, pp. 901–920, 2003.

[5] D. S. Bayard, "State-space approach to computing spacecraft pointing jitter," *Journal of guidance, control, and dynamics*, vol. 27, no. 3, pp. 426–433, 2004.

[6] J.-F. Magni, "User manual of the linear fractional representation toolbox," Tech. Rep. 10403.01, 2006.

[7] A. Saltelli, M. Ratto, T. Andres, F. Campolongo, J. Cariboni, D. Gatelli, M. Saisana, and S. Tarantola, *Global sensitivity analysis: the primer*. John Wiley & Sons, 2008.

[8] ESSB-HB-E-003 Working Group, "Esa pointing error engineering handbook ESSB-HB-E-003," ESA, Tech. Rep., 2011.

[9] C. Roos, F. Lescher, J.-M. Biannic, C. Döll, and G. Ferreres, "A set of μ-analysis based tools to evaluate the robustness properties of high-dimensional uncertain systems," in *2011 IEEE International Symposium on Computer-Aided Control System Design (CACSD)*, IEEE, 2011, pp. 644–649.

[10] T. Ott, W. Fichter, S. Bennani, and S. Winkler, "Precision pointing H_∞ control design for absolute, window-, and stability-time errors," *CEAS Space Journal*, vol. 4, no. 1, pp. 13–30, 2013.

[11] V. Preda, "Robust microvibration control and worst- case analysis for high pointing stability space missions," Ph.D. dissertation, Université de Bordeaux, 2018.

[12] European Cooperation for Space Standardization: Space Engineering, "ECSS-E-ST-60-20C Rev.2: Star sensor terminology and performance specification," 2019.

[13] F. Sanfedino, "Experimental validation of a high accuracy pointing system," Ph.D. dissertation, Toulouse, ISAE, 2019.

[14] M. Martin, F. Belien, A. Falke, and R. Förstner, "Robust performance analysis using H_2 -norm for quadcopter-based mobility on small bodies," in *2021 IEEE Aerospace Conference*, 2021, pp. 1–14.

[15] EUMETSAT. "Metop - second generation: Continuing high quality observations from polar orbit." (Jan. 2023), [Online]. Available: `https://www.eumetsat.int/metop-sg` (visited on 01/06/2023).

[16] C. Roos, "Systems modeling, analysis and control (smac) toolbox: An insight into the robustness analysis library," in *Proceedings of the IEEE Multiconference on Systems and Control*, available with the SMAC toolbox at http://w3.onera.fr/smac/smart, IEEE, Hyderabad, India: Hyderabad, India, August 2013, pp. 176–181.